Automatica 100 (2019) 123–134

Contents lists available at ScienceDirect

Automatica

journal homepage: www.elsevier.com/locate/automatica

Observer based path following for underactuated marine vessels in the presence of ocean currents: A global approach☆

Dennis Belleter [a], Mohamed Adlene Maghenem [b], Claudio Paliotta [a,*], Kristin Y. Pettersen [a]

[a] Centre for Autonomous Marine Operations and Systems (NTNU AMOS), Department of Engineering Cybernetics, Norwegian University of Science and Technology, NO7491 Trondheim, Norway
[b] University of California Santa Cruz, USA

ARTICLE INFO

Article history:
Received 1 October 2017
Received in revised form 24 June 2018
Accepted 26 October 2018
Available online 23 November 2018

Keywords:
Underactuated systems
Marine vehicles
Path following
Line-of-sight
Observer-based

ABSTRACT

In this paper a solution to the problem of following a curved path in the presence of a constant unknown ocean current disturbance is presented. We introduce a path variable that represents the curvilinear abscissa on the path, which is used to propagate the path-tangential reference frame. The proposed dynamic update law of the path variable is nonsingular and the guidance law is designed such that the vessel can reject constant unknown ocean currents by using an ocean current observer. It is shown that the closed-loop system composed of the guidance law, controller and observer provides globally asymptotically stable and locally exponentially stable path following errors. The sway velocity dynamics is analyzed and, under adequate conditions on the path curvature, it is shown that the dynamics is well behaved and the guidance law is well-defined. Simulations are presented to verify the theoretical findings.

1. Introduction

This paper considers curved path-following for underactuated marine vessels. While the literature for straight-line path following of underactuated marine vessels is, by now, well established even in the presence of unknown disturbances, see e.g. Aguiar and Hespanha (2007), Børhaug, Pavlov, Panteley, and Pettersen (2011), Do and Pan (2006), Lapierre and Soetanto (2007) and Oh and Sun (2010), the literature for curved paths is much less rich and has some lacks.

In the existing literature, we distinguish between local and global approaches to solving the path following problem for autonomous vehicles. In local approaches the path following problem is solved only when the vehicle starts in a certain neighborhood of the path. This last fact is due to the singularity that appears in the dynamics of the path variable that propagate the path-tangential reference frame, since it is designed to keep the vessel on the normal of the frame at the path variable abscissa (Micaelli & Samson, 1993). This method has the advantage of allowing faster convergence to the path compared to global approaches that solve the problem for all initial condition of the vehicle. The dynamics of the path variable, in this case, is used as a degree of freedom in the control design and is chosen to be nonsingular.

The local approaches for the case of underactuated marine vehicles have been inspired by the seminal works in Micaelli and Samson (1993) and Samson (1992) for the case of nonholonomic mobile robots. A first extension from mobile robots to the case of underactuated marine vessels appeared in Encarnaçao, Pascoal, and Arcak (2000), where the path parametrization from Micaelli and Samson (1993) is used to define the path-following problem, and a solution is presented using a nonlinear observer-based controller to incorporate the effects of an unknown but constant ocean current. Part of the closed-loop state is shown to be asymptotically stable and the zero dynamics is shown to be well behaved. Similar results for a 3D underactuated marine vessels are presented in Encarnaçao and Pascoal (2000). Another local result based on the path parametrization of Micaelli and Samson (1993) and Samson (1992) is provided in Do and Pan (2004), where only practical stability of the path-following errors is shown in the presence of environmental disturbances. Recently, in Maghenem, Belleter, Paliotta, and Pettersen (2017), we extended the latter result to guarantee exponential stability of the path following errors and to provide a complete analysis of the sway velocity.

A global approach to solve the path following problem under general curved paths for underactuated marine vehicles is

☆ This work was partly supported by the Research Council of Norway through the Centers of Excellence funding scheme, Project No. 223254 NTNU AMOS. The material in this paper was not presented at any conference. This paper was recommended for publication in revised form by Associate Editor Angelo Alessandri under the direction of Editor Thomas Parisini.

* Corresponding author.
E-mail addresses: dennisbelleter@gmail.com (D. Belleter), mmaghene@ucsc.edu (M.A. Maghenem), claudiopaliotta@ieee.org (C. Paliotta), kristin.y.pettersen@ntnu.no (K.Y. Pettersen).

https://doi.org/10.1016/j.automatica.2018.11.008
0005-1098/

presented in Lapierre and Soetanto (2007) and Lapierre, Soetanto, and Pascoal (2003) based on a result from the field of mobile robots in Soetanto, Lapierre, and Pascoal (2003). Solving this problem for this class of vehicles, offers the challenge of defining a controller which guarantees convergence of the vehicle to the path and at the same time gives boundedness of the sway velocity. In fact, when the vehicle moves along curved paths, the centrifugal effect causes a non-zero side velocity. In order to have a feasible motion of the vehicle, the controller has to guarantee a bounded sway velocity for curved paths. Note that for the case of straight line paths, the controller has to guarantee that the side velocity converges to zero since there is no centrifugal effect when following the path.

For the particular case of straight-line paths, a similar approach to Lapierre et al. (2003) is considered in Børhaug and Pettersen (2006) in which a look-ahead based steering law is used to guide the vehicle to the path. Stability of the path-following errors is shown using cascaded systems theory, and the zero dynamics are analyzed and shown to be well behaved. In Børhaug, Pavlov, and Pettersen (2008) ocean currents are taken into account by adding integral action to the steering law. The work in Børhaug et al. (2008) is reformulated in Caharija, Candeloro, Pettersen, and Sørensen (2012) and Caharija, Pettersen, Gravdahl, and Børhaug (2012) using relative velocities. Experimental results are obtained in Caharija et al. (2016). See also Li, Sun, and Oh (2009), where a control design for straight-line paths has been validated by experiments. However in this work the sway dynamics are neglected in the control design procedure and stability analysis. Furthermore, for the particular case of circles and paths made of straight-line sections connecting way points, line-of-sight guidance laws are presented in Breivik and Fossen (2004) and Fossen, Breivik, and Skjetne (2003), respectively. In Breivik and Fossen (2004) the vessel is regulated to the tangent of its projection on the circle. An extension to the three dimensional case is given in Breivik and Fossen (2005a, b). However, these works do not consider environmental disturbances.

For the case of general curved paths, we notice that a non-complete analysis of closed-loop dynamics has been provided in most of the existing literature. Specifically, the sway dynamics is not analyzed and the existence and boundedness of the control input is not guaranteed (Lapierre & Soetanto, 2007; Lapierre et al., 2003; Moe, Caharija, Pettersen, & Schjølberg, 2014). At the exception of Paliotta et al. (2018), where a different approach to the trajectory tracking and path following problems is proposed. The approach presented in Paliotta et al. (2018) is based on a different choice of the output of the system, the so called hand position point. Then the authors apply an input–output linearizing controller in order to make the new output converge to the desired path. However, the controller presented in Paliotta et al. (2018) is not applicable if the same output for the system as in Lapierre and Soetanto (2007), Lapierre et al. (2003) and Moe et al. (2014) is chosen. In this paper, we provide a rigorous approach by keeping the traditional choice of the pivot point as output of the system and by modifying the control structure proposed in Moe et al. (2014). These modifications allow us to guarantee the global asymptotic stability of the path following errors. Moreover, we derive sufficient conditions on the path curvature that allow us to prove the existence of the control law and the boundedness of the sway velocity. This is achieved by considering a global parametrization of the general curved path in order to solve the problem using a combination of an ocean current observer and a controller based on a *line-of-sight-like* guidance. We consider underactuated vehicles, in particular, vehicles which do not have sway actuation. The guidance based controller proposed in this paper is said to be line-of-sight-like since it adopts a time-varying look-ahead distance depending on the path-following error. The time-varying look-ahead distance is modified compared to the one in Moe et al. (2014), and it is shown that a new dependency on the path-following errors is crucial to prove boundedness of the sway velocity, which is the best behavior we can achieve for the zero dynamics in the case of general curved paths. It should be noted that these modifications are not merely an extension but are necessary conditions for the validity of stability results for the problem under consideration. To the best of our knowledge, such a result is unique in the literature of underactuated marine vehicles. Furthermore in Moe et al. (2014) the controller for the yaw rate dynamics used signals that dependent on the unknown ocean current. Therefore the controller could not be implemented. We specifically address this issue and derive a controller for the yaw rate dynamics that depends only on known signals.

The outline of the paper is as follows. In Section 2 the vessel model is given. The path-following problem and the chosen path parametrization are introduced in Section 3. Section 5 presents the ocean current observer that is used together with the guidance law and controllers. The closed-loop system is then formulated and analyzed in Section 6. A simulation case study is presented in Section 7 and conclusions are given in Section 8.

2. Vehicle model

In this section we introduce the vehicle's model given in Fossen (2011, p. 152–157). However, in the simulation section we explain why we use $u_{rd} = 5$ m/s in the case studies. This model can be used to describe an autonomous surface vessel or an autonomous underwater vehicle moving in the plane. The dynamics of the vehicle is:

$$\dot{\eta} = R(\psi)\nu_r + V \tag{1a}$$

$$M\dot{\nu}_r + C(\nu_r)\nu_r + D\nu_r = Bf \tag{1b}$$

where $\eta \triangleq [x, y, \psi]^T$ describes the position of the center of gravity and the orientation of the vehicle with respect to the inertial frame, $\nu_r \triangleq [u_r, v_r, r]^T$ contains the surge, the sway and the yaw velocities respectively, M is the mass matrix, $C(\nu_r)$ is the Coriolis matrix, D is the damping matrix, B is the thrust allocation matrix, and $f \triangleq [T_u, T_r]$ is the vector of control inputs composed by the surge thrust and the rudder angle inputs T_u and T_r, respectively.

For port-starboard symmetric vehicles, the matrices (M, B, C, D) have the following structure:

$$M \triangleq \begin{bmatrix} m_{11} & 0 & 0 \\ 0 & m_{22} & m_{23} \\ 0 & m_{32} & m_{33} \end{bmatrix}; B \triangleq \begin{bmatrix} b_{11} & 0 \\ 0 & b_{22} \\ 0 & b_{32} \end{bmatrix}; \tag{2a}$$

$$C \triangleq \begin{bmatrix} 0 & 0 & -m_{22}v_r - m_{23}r \\ 0 & 0 & m_{11}u_r \\ m_{22}v_r + m_{23}r & -m_{11}u_r & 0 \end{bmatrix}; \tag{2b}$$

$$D \triangleq \begin{bmatrix} d_{11} & 0 & 0 \\ 0 & d_{22} & d_{23} \\ 0 & d_{32} & d_{33} \end{bmatrix}. \tag{2c}$$

It is worth noting that the model (1) is valid for low speed motion, for which the damping can be assumed to be linear. Specifically, at low speed the non-linear damping effects can be neglected (Fossen, 2011, p. 152–157). In the simulations in this paper, we use a model from Caharija (2014) in which the damping is linear up to ± 7 [m/s]. Furthermore, since $f \in \mathbf{R}^2$, the vehicle is under-actuated in the work space $\mathbf{R}^3$. This latter fact implies that the vehicle is not directly actuated in the sway direction, that is, sideways. Moreover, given the structure of the matrix B in (2a), it is easy to see that the control input in yaw T_r, indirectly affects the sway direction. However, according to Fredriksen and Pettersen (2004), for port-starboard symmetric vehicles, it is always possible to apply a change of coordinates such that the model (1), can be expressed with respect to a coordinate frame positioned at the pivot point

instead of at the center of gravity. The pivot point lies along the center line of the vehicle, ahead of the center of gravity and always exists for port-starboard vehicles (Fredriksen & Pettersen, 2004), and in this point the yaw control does not affect the sway motion. Hence, the dynamical model with the body-fixed frame positioned at the pivot point is the following:

$$\dot{x} = u_r \cos(\psi) - v_r \sin(\psi) + V_x \tag{3a}$$
$$\dot{y} = u_r \sin(\psi) + v_r \cos(\psi) + V_y \tag{3b}$$
$$\dot{\psi} = r \tag{3c}$$
$$\dot{u}_r = F_{u_r}(v_r, r) - \tfrac{d_{11}}{m_{11}} u_r + \tau_u \tag{3d}$$
$$\dot{v}_r = X(u_r) r + Y(u_r) v_r \tag{3e}$$
$$\dot{r} = F_r(u_r, v_r, r) + \tau_r. \tag{3f}$$

where τ_u and τ_r are, respectively, the surge force and the yaw torque input. The functions $X(u_r)$, $Y(u_r)$, F_u, and F_r are given by

$$F_{u_r}(v_r, r) \triangleq \tfrac{1}{m_{11}}(m_{22} v_r + m_{23} r) r \tag{4a}$$
$$X(u_r) \triangleq \tfrac{m_{23}^2 - m_{11} m_{33}}{m_{22} m_{33} - m_{23}^2} u_r + \tfrac{d_{33} m_{23} - d_{23} m_{33}}{m_{22} m_{33} - m_{23}^2} \tag{4b}$$
$$Y(u_r) \triangleq \tfrac{(m_{22} - m_{11}) m_{23}}{m_{22} m_{33} - m_{23}^2} u_r - \tfrac{d_{22} m_{33} - d_{32} m_{23}}{m_{22} m_{33} - m_{23}^2} \tag{4c}$$
$$F_r(\cdot) \triangleq \tfrac{m_{23} d_{22} - m_{22}(d_{32} + (m_{22} - m_{11}) u_r)}{m_{22} m_{33} - m_{23}^2} v_r + \tfrac{m_{23}(d_{23} + m_{11} u_r) - m_{22}(d_{33} + m_{23} u_r)}{m_{22} m_{33} - m_{23}^2} r. \tag{4d}$$

Note that the functions $X(u_r)$ and $Y(u_r)$ are linear functions of the velocity. The kinematic variables are illustrated in Fig. 1. The ocean current satisfies the following assumption.

Assumption 1. The ocean current is assumed to be a constant in time, uniform in space, and irrotational with respect to the inertial frame, i.e. $\boldsymbol{V_c} \triangleq [V_x, V_y, 0]^T$. Furthermore, there exists a constant $V_{\max} > 0$ such that $\|\boldsymbol{V_c}\| = \sqrt{V_x^2 + V_y^2} \leq V_{\max}$.

We consider a range of values of the desired surge velocity u_{rd} such that the following assumption holds.

Assumption 2. It is assumed that $Y(u_r)$ satisfies

$$Y(u_r) \leq -Y_{\min} < 0, \ \forall u_r \in [-V_{\max}, u_{rd}],$$

i.e. $Y(u_r)$ is negative for the range of desired velocities considered.

Additionally we assume that the following assumption holds.

Assumption 3. It is assumed that $u_{rd}(t)$ is $\mathcal{C}^1$ and satisfies $u_{rd}(t) > 2V_{\max}\ \forall t$, i.e. the desired relative velocity of the vessel is larger than twice the maximum value of the ocean current.

Assumption 3 assures that the vessel has enough propulsion power to overcome the ocean current affecting it. The factor two in Assumption 3 adds some extra conservativeness to bound the solutions of the ocean current observer, and this is discussed further in Section 5.

3. Problem definition

The objective in global path-following problems is to make each trajectory of the controlled vehicle converge to a desired trajectory describing a smooth path P regardless of the vehicle's initial location. For an underactuated vehicle, the path following task can be achieved by positioning the vehicle on the path with a total speed $u_t \triangleq \sqrt{u_r^2 + v_r^2}$ (see Fig. 1) that is tangential to the path. However, this approach restricts the initial location of the vehicle to be on the path. To have a more general result in terms of

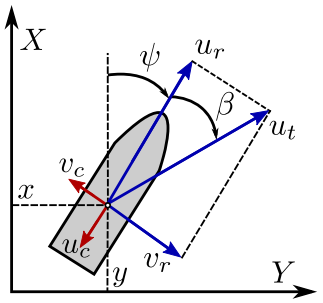

Fig. 1. Definition of the vehicle state variables.

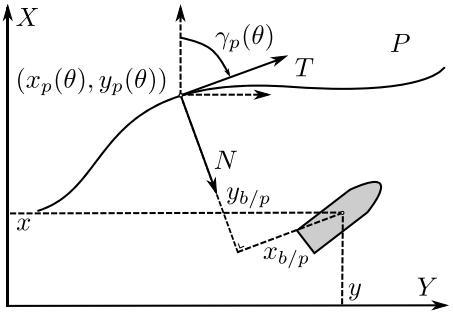

Fig. 2. Definition of the path.

both attractivity and invariance of the path, we introduce adequate path-following errors. The path-following errors correspond to the error between the vehicle and a point moving on the path. To do so, we parametrize the path P using a path variable θ. Moreover, for each point on the path, $(x_p(\theta), y_p(\theta)) \in P$, we introduce a path-tangential frame as illustrated in Fig. 2. Hence, the path-following errors expressed in the tangential frame and denoted by $\boldsymbol{p}_{b/p} \triangleq [x_{b/p}, y_{b/p}]^T$ take the following form:

$$\begin{bmatrix} x_{b/p} \\ y_{b/p} \end{bmatrix} = \begin{bmatrix} \cos(\gamma_p(\theta)) & \sin(\gamma_p(\theta)) \\ -\sin(\gamma_p(\theta)) & \cos(\gamma_p(\theta)) \end{bmatrix} \begin{bmatrix} x - x_p(\theta) \\ y - y_p(\theta) \end{bmatrix} \tag{5}$$

where $\gamma(\theta)$ is the angle of the path with respect to the inertial X-axis.

The time derivative of the angle $\gamma(\theta)$ is given by $\dot{\gamma}(\theta) = \kappa(\theta)\dot{\theta}$ where $\kappa(\theta)$ is the curvature of P at θ. The path-following error is expressed by $x_{b/p}$ and $y_{b/p}$ which are the relative positions between the path frame and the body frame expressed along the axes of the path frame. Hence, $x_{b/p}$ is the position of the vehicle along the path-frame tangential axis and $y_{b/f}$ is the position of the vehicle along the path-frame normal axis. That is, the path-following problem is solved if we regulate both $x_{b/p}$ and $y_{b/p}$ to zero when $\boldsymbol{p}_p(\theta) \triangleq (x_p(\theta), y_p(\theta))$ describes the path P parametrized by θ.

The dynamics of the error coordinates introduced in (5) is computed by substitute (3a)–(3c) in the derivative of (5). After some rearrangements and basic trigonometric relations we obtain:

$$\dot{x}_{b/p} = u_t \cos(\chi - \gamma_p) - \dot{\theta}(1 - \kappa(\theta) y_{b/p}) + V_T \tag{6a}$$
$$\dot{y}_{b/p} = u_t \sin(\chi - \gamma_p) + V_N - \kappa(\theta)\dot{\theta} x_{b/p} \tag{6b}$$

where $\chi \triangleq \psi + \beta$ and $\beta \triangleq \arctan(v_r/u_r)$ are the course and the side-slip angles respectively (see Fig. 1), $V_T \triangleq V_x \cos(\gamma_p(\theta)) + V_y \sin(\gamma_p(\theta))$ and $V_N \triangleq V_y \cos(\gamma_p(\theta)) - V_x \sin(\gamma_p(\theta))$ are the ocean current components in the tangential direction and normal direction of the path-tangential reference frame respectively.

4. Path parametrization

As proposed in Lapierre and Soetanto (2007) we can use the update law of the path variable as an extra degree of freedom in the controller design. In particular, the propagation speed of the frame is used to obtain the desired behavior of the $x_{b/p}$ dynamics. We choose

$$\dot{\theta} = u_t \cos(\chi - \gamma_p(\theta)) + k_x f_\theta(x_{b/p}, y_{b/p}) + V_T \tag{7}$$

where $k_x > 0$ is a control gain for the convergence of $x_{b/p}$ and $f_\theta(x_{b/p}, y_{b/p})$ is a function to be designed later satisfying $f_\theta(x_{b/p}, y_{b/p})$
$x_{b/p} > 0$. Consequently, when substituting (7) in (6a) we obtain

$$\dot{x}_{b/p} = -k_x f_\theta(x_{b/p}, y_{b/p}) + \dot{\theta}\kappa(\theta) y_{b/p}. \tag{8}$$

For the case where the current is unknown we need to replace V_T by its estimate $\hat{V}_T$, and the update law becomes

$$\dot{\theta} = u_t \cos(\chi - \gamma_p(\theta)) + k_x f_\theta(x_{b/p}, y_{b/p}) + \hat{V}_T \tag{9}$$

Substituting this revised update law into (6) results in

$$\dot{x}_{b/p} = -k_x f_\theta(x_{b/p}, y_{b/p}) + \dot{\theta}\kappa(\theta) y_{b/p} + \tilde{V}_T \tag{10}$$

$$\dot{y}_{b/p} = u_t \sin(\chi - \gamma_p(\theta)) + V_N - x_{b/p}\kappa(\theta)\dot{\theta} \tag{11}$$

where $\tilde{V}_T \triangleq V_T - \hat{V}_T$. Note that, as opposed to Maghenem et al. (2017), the parametrization (9) does not decouple (10) from (11). Consequently, since (10) depends on $y_{b/p}$, the state $x_{b/p}$ does not converge independently from $y_{b/p}$ and both $x_{b/p}$ and $y_{b/p}$ will have to be regulated to zero using the surge and yaw rate controllers. Moreover, note that although this parametrization has the advantage over (Maghenem et al., 2017) that the update law can be well defined on the entire state space, the path-following error is here not defined as the shortest distance to the path since the vehicle is not necessarily on the normal.

5. Controllers, observer, and guidance

In this section we design the two control laws, τ_u and τ_r, and the ocean current estimator that are used to achieve path-following. In the first subsection we present the velocity control law τ_u. The second subsection presents the ocean current observer. The third subsection presents the guidance law to be used.

5.1. Surge velocity control

The velocity control law is a feedback-linearizing P-controller that is used to drive the relative surge velocity to the desired $u_{rd}(t)$ and is given by

$$\tau_u = -F_{u_r}(v_r, r) + \dot{u}_{rd} + \frac{d_{11}}{m_{11}} u_{rd} - k_u(u_r - u_{rd}) \tag{12}$$

where $k_u > 0$ is a constant controller gain. It is straightforward to verify that (12) ensures global exponential tracking of the desired velocity. In particular, when (12) is substituted in (3d) we obtain

$$\dot{\tilde{u}}_r = -k_u(u_r - u_{rd}) = -k_u \tilde{u}_r \tag{13}$$

where $\tilde{u}_r \triangleq u_r - u_{rd}$. Consequently, the velocity error dynamics are described by a stable linear system, which assures exponential tracking of the desired velocity u_{rd}.

5.2. Ocean current estimator

In this section we present the ocean current observer and show that for constant ocean currents the estimation errors are globally exponentially stable. Moreover, for an appropriate choice of the initial conditions we have

$$\|\hat{V}_N(t)\| < u_{rd}(t), \text{ if } 2V_{\max} < u_{rd}(t), \ \forall t \geq 0$$

where $\hat{V}_N(t)$ is the estimate of $V_N(t)$.

We will use the ocean current estimator introduced in Moe et al. (2014) and used in Maghenem et al. (2017). This observer provides the estimate of the ocean current needed to implement (9) and the guidance law developed in the next subsection. Rather than estimating the time-varying current components in the path frame V_T and V_N, the observer is used to estimate the constant ocean current components in the inertial frame V_x and V_y. The observer from Aguiar and Pascoal (2007) is based on the kinematic equations of the vehicle, i.e. (3a) and (3b), and requires measurements of the vehicle's x and y position in the inertial frame. The observer is formulated as

$$\dot{\hat{x}} = u_r \cos(\psi) - v_r \sin(\psi) + \hat{V}_x + k_{x_1}\tilde{x} \tag{14a}$$

$$\dot{\hat{y}} = u_r \sin(\psi) + v_r \cos(\psi) + \hat{V}_y + k_{y_1}\tilde{y} \tag{14b}$$

$$\dot{\hat{V}}_x = k_{x_2}\tilde{x} \tag{14c}$$

$$\dot{\hat{V}}_y = k_{y_2}\tilde{y} \tag{14d}$$

where $\tilde{x} \triangleq x - \hat{x}$ and $\tilde{y} \triangleq y - \hat{y}$ are the positional errors and $k_{x_1}, k_{x_2}, k_{y_1}$, and k_{y_2} are constant positive gains. Consequently, the estimation error dynamics are given by

$$\begin{bmatrix} \dot{\tilde{x}} \\ \dot{\tilde{y}} \\ \dot{\tilde{V}}_x \\ \dot{\tilde{V}}_y \end{bmatrix} = \begin{bmatrix} -k_{x_1} & 0 & 1 & 0 \\ 0 & -k_{y_1} & 0 & 1 \\ -k_{x_2} & 0 & 0 & 0 \\ 0 & -k_{y_2} & 0 & 0 \end{bmatrix} \begin{bmatrix} \tilde{x} \\ \tilde{y} \\ \tilde{V}_x \\ \tilde{V}_y \end{bmatrix} \tag{15}$$

which is a linear system with negative eigenvalues. Hence, the observer error dynamics are globally exponentially stable at the origin. Note that this implies that also $\hat{V}_T$ and $\hat{V}_N$ go to V_T and V_N respectively with exponential convergence since it holds that

$$\hat{V}_T = \hat{V}_x \cos(\gamma(\theta)) + \hat{V}_y \sin(\gamma(\theta)) \tag{16a}$$

$$\hat{V}_N = -\hat{V}_x \sin(\gamma(\theta)) + \hat{V}_y \cos(\gamma(\theta)). \tag{16b}$$

For implementation of the controllers it is desired that $\|\hat{V}_N(t)\| < u_{rd}(t)\, \forall t$. To achieve this we first choose the initial conditions of the estimator as

$$[\hat{x}(t_0), \hat{y}(t_0), \hat{V}_x(t_0), \hat{V}_y(t_0)]^T = [x(t_0), y(t_0), 0, 0]^T. \tag{17}$$

Consequently, the initial estimation error is given by

$$[\tilde{x}(t_0), \tilde{y}(t_0), \tilde{V}_x(t_0), \tilde{V}_y(t_0)]^T = [0, 0, V_x, V_y]^T \tag{18}$$

which has a norm smaller than or equal to $V_{\max}$ according to Assumption 1. Now consider the function

$$W(t) = \tilde{x}^2 + \tilde{y}^2 + \frac{1}{k_{x_2}}\tilde{V}_x^2 + \frac{1}{k_{y_2}}\tilde{V}_y^2 \tag{19}$$

which has the following time derivative

$$\dot{W}(t) = -2k_{x_1}\tilde{x}^2 - 2k_{y_1}\tilde{y}^2 \leq 0. \tag{20}$$

This implies that $W(t) \leq \|W(t_0)\|$. From our choice of initial conditions we know that

$$\|W(t_0)\| = \frac{V_x^2}{k_{x_2}} + \frac{V_y^2}{k_{y_2}} \leq \frac{1}{\min(k_{x_2}, k_{y_2})} V_{\max}^2. \tag{21}$$

Moreover, it is straightforward to verify

$$\frac{1}{\max(k_{x_2}, k_{y_2})}\|\tilde{\boldsymbol{V}}_c(t)\|^2 \leq W(t). \tag{22}$$

Combining the observations given above we obtain

$$\frac{1}{\max(k_{x_2}, k_{y_2})}\|\tilde{\boldsymbol{V}}_c(t)\|^2 \leq \frac{1}{\min(k_{x_2}, k_{y_2})}V_{\max}^2. \tag{23}$$

Consequently, we obtain

$$\begin{aligned}\|\tilde{\boldsymbol{V}}_c(t)\| &\leq \sqrt{\frac{\max(k_{x_2}, k_{y_2})}{\min(k_{x_2}, k_{y_2})}}V_{\max} \\ &< \sqrt{\frac{\max(k_{x_2}, k_{y_2})}{\min(k_{x_2}, k_{y_2})}}u_{rd}(t),\ \forall t,\end{aligned} \tag{24}$$

which implies that if the gains are chosen as $k_{x_2} = k_{y_2}$ we have

$$\|\hat{V}_N\| \leq 2V_{\max} \leq u_{rd}(t),\ \forall t. \tag{25}$$

Hence, $\|\hat{V}_N\| < u_{rd}(t),\ \forall t$ if $2V_{\max} < u_{rd}(t),\ \forall t$.

Remark 1. The bound $u_{rd}(t) > 2V_{\max},\ \forall t$, is only required when deriving the bound on the solutions of the observer. In particular, it is required to guarantee that $\|\hat{V}_N\| < u_{rd}(t),\ \forall t$. For the rest of the analysis it suffices that $V_{\max} < u_{rd},\ \forall t$. Therefore, if the more conservative bound $2V_{\max} < u_{rd},\ \forall t$ is not satisfied, the observer can be changed to an observer that allows explicit bounds on the estimate $\hat{V}_N$, e.g. the observer developed in Narendra and Annaswamy (1987), rather than an observer that only provides a bound on the error $\tilde{\boldsymbol{V}}_c$ as is the case here. For practical purposes, the estimate can also be saturated such that $\|\hat{V}_N\| < u_{rd},\ \forall t$, which is the approach taken in Moe et al. (2014). However, in the theoretical analysis of the yaw controller we use derivatives of $\hat{V}_N$ which will be discontinuous when saturation is applied.

5.3. Guidance for global parametrization

When using the global parametrization we can define one guidance law that can be used everywhere. As in Moe et al. (2014) we choose a line-of-sight like guidance law of the form:

$$\psi_d = \gamma(\theta) - \operatorname{atan}\left(\frac{v_r}{u_{rd}}\right) - \operatorname{atan}\left(\frac{y_{b/p}+g}{\Delta(\boldsymbol{p}_{b/p})}\right). \tag{26}$$

The guidance law consists of three terms. The first term is a feed-forward of the angle of the path with respect to the inertial frame. The second part is the desired side-slip angle, i.e. the angle between the surge velocity and the total speed when $u_r \equiv u_{rd}$. This side-slip angle is used to make the vehicle's total speed tangential to the path when the sway velocity is non-zero. The third term is a line-of-sight (LOS) term that is intended to steer the vehicle to the path, where g is a term dependent on the ocean current. The choice of g provides an extra design freedom to compensate for the component of the ocean current along the normal axis V_N.

The term $\Delta(\boldsymbol{p}_{b/p})$ is the look-ahead distance. The look-ahead distance has a constant part and a part that depends on the path-following error $\boldsymbol{p}_{b/p}$, i.e. the distance between the current position of the vehicle and the point on the path defined by the current value of θ.

When we substitute (26) in (11) we obtain

$$\begin{aligned}\dot{y}_{b/p} &= u_{td}\sin\left(\psi_d + \tilde{\psi} + \beta_d - \gamma_p(\theta)\right) + V_N \\ &\quad - x_{b/p}\kappa(\theta)\dot{\theta} + \tilde{u}_r\sin(\psi - \gamma_p(\theta)) \\ &= -\frac{u_{td}(y_{b/p}+g)}{\sqrt{(y_{b/p}+g)^2+\Delta^2}} - x_{b/p}\dot{\gamma}_p(\theta) \\ &\quad + V_N + G_1(\tilde{\psi}, \tilde{u}_r, g, \psi_d, y_{b/p}, u_{td})\end{aligned} \tag{27}$$

where $G_1(\cdot)$ is a perturbing term given by

$$\begin{aligned}G_1(\cdot) &= u_{td}\left[1-\cos(\tilde{\psi})\right]\sin\left(\arctan\left(\frac{y_{b/p}+g}{\Delta}\right)\right) \\ &\quad + \tilde{u}_r\sin(\psi - \gamma_p(\theta)) \\ &\quad + u_{td}\cos\left(\arctan\left(\frac{y_{b/p}+g}{\Delta}\right)\right)\sin(\tilde{\psi}).\end{aligned} \tag{28}$$

Note that $G_1(\cdot)$ satisfies

$$G_1(0, 0, g, \psi_d, y_{b/p}, u_{td}) = 0 \tag{29a}$$

$$\|G_1(\tilde{\psi}, \tilde{u}_r, \psi_d, y_{b/p}, u_{td})\| \leq \zeta(u_{td})\|[\tilde{\psi}, \tilde{u}_r]^T\| \tag{29b}$$

where $\zeta(u_{td}) > 0$, which shows that $G_1(\cdot)$ is zero when the perturbing variables are zero and that it has maximal linear growth in the perturbing variables.

To compensate for the ocean current component V_N, the variable g is now chosen to satisfy the equality

$$u_{td}\frac{g}{\sqrt{\Delta^2+(y_{b/p}+g)^2}} = \hat{V}_N \tag{30}$$

which is a choice inspired by Moe et al. (2014). In order for g to satisfy the equality above, it should be the solution of the following second order equality:

$$\underbrace{(u_{td}^2 - \hat{V}_N^2)}_{-a}\left(\frac{g}{\hat{V}_N}\right)^2 = \underbrace{\Delta^2 + y_{b/p}^2}_{c} + 2\underbrace{y_{b/p}\hat{V}_N}_{b}\left(\frac{g}{\hat{V}_N}\right)$$

hence, we choose g to be

$$g = \hat{V}_N\frac{b+\sqrt{b^2-ac}}{-a} \tag{31}$$

which has the same sign as $\hat{V}_N$ and is well defined for $(u_{rd}^2 - \hat{V}_N^2) = -a > 0$. Substituting this in (27) gives

$$\begin{aligned}\dot{y}_{b/p} &= -u_{td}\frac{y_{b/p}}{\sqrt{(y_{b/p}+g)^2+\Delta^2}} - x_{b/p}\dot{\gamma}_p(\theta) \\ &\quad + \tilde{V}_N + G_1(\tilde{\psi}, \tilde{u}, \psi_d, y_{b/p}, u_{td}).\end{aligned} \tag{32}$$

By choosing $\dot{\theta}$ to be:

$$\dot{\theta} = u_t\cos(\psi + \beta - \gamma_p(\theta)) + \frac{k_\delta x_{b/p}}{\sqrt{1+x_{b/p}^2}} + \hat{V}_T \tag{33}$$

and substituting (33) in (10), we obtain:

$$\dot{x}_{b/p} = -k_\delta\frac{x_{b/p}}{\sqrt{1+x_{b/p}^2}} + \dot{\theta}\kappa(\theta)y_{b/p} + \tilde{V}_T \tag{34}$$

where $k_\delta > 0$. We see from (34) that by the choice of $\dot{\theta}$, we introduce a stabilizing term to the tangential error dynamics by appropriately controlling the propagation of our path-tangential frame.

The derivative of (26) is given by

$$\begin{aligned}\dot{\psi}_d &= \kappa(\theta)\dot{\theta} + \frac{y_{b/p}+g}{\Delta^2+(y_{b/p}+g)^2}\frac{\partial\Delta}{\partial\boldsymbol{p}_{b/p}}\dot{\boldsymbol{p}}_{b/p} \\ &\quad - \frac{\dot{v}_r u_{rd} - \dot{u}_{rd}v_r}{u_{rd}^2+v_r^2} - \frac{\Delta(\dot{y}_{b/p}+\dot{g})}{\Delta^2+(y_{b/f}+g)^2}\end{aligned} \tag{35}$$

with

$$\dot{g} = \dot{\hat{V}}_N\frac{b+\sqrt{b^2-ac}}{-a} + \frac{\partial g}{\partial a}\dot{a} + \frac{\partial g}{\partial b}\dot{b} + \frac{\partial g}{\partial c}\dot{c}. \tag{36}$$

The expression for $\dot{\psi}_d$ contains terms depending on $\dot{y}_{b/p}$ and $\dot{x}_{b/p}$ which depend on $\tilde{V}_N$ and $\tilde{V}_T$, respectively. Consequently, $\dot{\psi}_d$

depends on unknown variables and cannot be used to implement the yaw rate controller. This was not considered in Moe et al. (2014) where the proposed controller contained both $\dot{\psi}_d$ and $\ddot{\psi}_d$.

Moreover, from (35) we see that $\dot{\psi}_d$ contains $\dot{v}_r$, which depends on $r = \dot{\psi}$. Therefore, the yaw rate error $\dot{\tilde{\psi}} \triangleq \dot{\psi} - \dot{\psi}_d$ grows with $\dot{\psi}$, which leads to a necessary condition for a well defined yaw rate error. In particular, the dependence on $r = \dot{\psi}$ becomes clear when we write out the yaw rate error dynamics:

$$\begin{aligned}\dot{\tilde{\psi}} =& r\left[1+\frac{X(u_r)u_{rd}}{u_{rd}^2+v_r^2}-\frac{2v_rX(u_r)\Delta}{\Delta^2+\left(y_{b/p}+g\right)^2}\frac{\partial g}{\partial a}\right]\\ &-\kappa(\theta)\dot{\theta}+\frac{Y(u_r)v_ru_{rd}-\dot{u}_{rd}v_r}{u_{rd}^2+v_r^2}\\ &+\frac{2\Delta}{\Delta^2+\left(y_{b/p}+g\right)^2}\left[\dot{\hat{V}}_N\frac{b+\sqrt{b^2-ac}}{-2a}\right.\\ &+\frac{\partial g}{\partial a}\left(\hat{V}_N\dot{\hat{V}}_N-u_{rd}\dot{u}_{rd}-v_rY(u_r)v_r\right)\\ &+\frac{\partial g}{\partial b}\dot{\hat{V}}_Ny_{b/p}+\left[\frac{1}{2}+\frac{\partial g}{\partial c}y_{b/p}+\frac{\partial g}{\partial b}\hat{V}_N\right]\dot{y}_{b/p}\\ &\left.+\frac{\partial g}{\partial c}\Delta\left[\frac{\partial\Delta}{\partial x_{b/p}}\dot{x}_{b/p}+\frac{\partial\Delta}{\partial y_{b/p}}\dot{y}_{p/f}\right]\right]\\ &-\frac{y_{b/p}+g}{\Delta^2+(y_{b/p}+g)^2}\left[\frac{\partial\Delta}{\partial x_{b/p}}\dot{x}_{b/p}+\frac{\partial\Delta}{\partial y_{b/p}}\dot{y}_{b/p}\right]\\ \triangleq& C_r(\cdot)r+f_\psi(x_{b/p},y_{b/p},u_r,v_r,\theta).\end{aligned}\tag{37}$$

Since $\dot{\psi}_d$ depends on the unknown signal $\tilde{V}_N$ we cannot choose $r_d = \dot{\psi}_d$. To define an expression for r_d without requiring the knowledge of $\tilde{V}_N$, we define $r_d = f_\psi(x_{b/p}, y_{b/p}, u_r, v_r, \theta)/C_r$. Consequently, we have the following necessary condition for the existence of our controller:

Condition 1. *It should hold that*

$$C_r \triangleq 1+\left[\frac{X(u_r)u_{rd}}{u_{rd}^2+v_r^2}-\frac{2X(u_r)v_r\Delta}{\Delta^2+\left(y_{b/p}+g\right)^2}\frac{\partial g}{\partial a}\right]\tag{38}$$

is larger than zero such that the yaw rate controller is well defined for all time.

Remark 2. The condition above can be verified for any positive velocity, for the vehicles that we have model parameters for. Note that for most vehicles this condition is verifiable since standard vehicle design practices will result in similar properties of the function $X(u_r)$. Besides having a lower bound greater then zero, C_r is also upper-bounded since the term between brackets can be verified to be bounded in its arguments.

As discussed above, since $\dot{\psi}_d$ depends on the unknown signal $\tilde{V}_N$, we cannot choose $r_d = \dot{\psi}_d$. To define an expression for r_d without requiring the knowledge of $\tilde{V}_N$ we use (38) to define

$$\begin{aligned}r_d =& -C_r^{-1}\left[\kappa(\theta)\left(u_t\cos(\chi-\gamma_p)+\frac{k_\delta x_{b/p}}{\sqrt{1+x_{b/p}^2}}+\hat{V}_T\right)\right.\\ &+\frac{Y(u_r)v_ru_{rd}-\dot{u}_{rd}v_r}{u_{rd}^2+v_r^2}+\frac{\Delta}{\Delta^2+(y_{b/p}+g)^2}\left[\dot{\hat{V}}_N\frac{b+\sqrt{b^2-ac}}{-a}\right.\\ &+2\frac{\partial g}{\partial b}\dot{\hat{V}}_Ny_{b/p}+2\frac{\partial g}{\partial a}\left(\hat{V}_N\dot{\hat{V}}_N-u_{rd}\dot{u}_{rd}\right.\\ &\left.\left.\left.-Y(u_r)v_r^2\right)+\left[1+\frac{\partial g}{\partial c}2y_{b/p}+\frac{\partial g}{\partial b}2\hat{V}_N\right]\times\right.\right.\\ &\times\left(\frac{-u_{td}y_{b/p}}{\sqrt{\Delta^2+(y_{b/p}+g)^2}}+G_1-x_{b/p}\kappa(\theta)\dot{\theta}\right)\\ &+\frac{\partial g}{\partial c}2\Delta\left[\frac{\partial\Delta}{\partial x_{b/p}}\left(\frac{-k_\delta x_{b/p}}{\sqrt{1+x_{b/p}^2}}+y_{b/p}\kappa(\theta)\dot{\theta}\right)\right.\\ &\left.\left.+\frac{\partial\Delta}{\partial y_{b/p}}\left(\frac{-u_{td}y_{b/p}}{\sqrt{\Delta^2+(y_{b/p}+g)^2}}+G_1-x_{b/p}\kappa(\theta)\dot{\theta}\right)\right]\right]\\ &-\frac{y_{b/p}+g}{\Delta^2+(y_{b/p}+g)^2}\left[\frac{\partial\Delta}{\partial x_{b/p}}\left(\frac{-k_\delta x_{b/p}}{\sqrt{1+x_{b/p}^2}}+y_{b/p}\kappa(\theta)\dot{\theta}\right)\right.\\ &\left.+\frac{\partial\Delta}{\partial y_{b/p}}\left(\frac{-u_{td}y_{b/p}}{\sqrt{\Delta^2+(y_{b/p}+g)^2}}+G_1-x_{b/p}\kappa(\theta)\dot{\theta}\right)\right]\end{aligned}\tag{39}$$

with,

$$\begin{aligned}\dot{\hat{V}}_N =& \dot{\hat{V}}_y\cos(\gamma_p(\theta))-\dot{\hat{V}}_x\sin(\gamma_p(\theta))+\kappa(\theta)\hat{V}_T^2\\ &-\hat{V}_T\kappa(\theta)\left(u_t\cos(\chi-\gamma_p(\theta))+\frac{k_\delta x_{b/p}}{\sqrt{1+x_{b/p}^2}}\right).\end{aligned}\tag{40}$$

Notice that (39) is equivalent to (26), but without the terms depending on the unknowns $\tilde{V}_x$ and $\tilde{V}_y$ that cannot be used in the control inputs. If we substitute (39) in (37) and use $\tilde{r} \triangleq r - r_d$, we obtain

$$\begin{aligned}\dot{\tilde{\psi}} =& C_r\tilde{r}+\frac{2\Delta\left[\frac{1}{2}+\frac{\partial g}{\partial c}y_{b/p}+\frac{\partial g}{\partial b}\hat{V}_N\right]}{\Delta^2+\left(y_{b/p}+g\right)^2}\tilde{V}_N\\ &+\frac{2\Delta^2\partial g/\partial c-(y_{b/p}+g)}{\Delta^2+\left(y_{b/p}+g\right)^2}\frac{\partial\Delta}{\partial\boldsymbol{p}_{b/p}}\begin{bmatrix}\tilde{V}_T\\ \tilde{V}_N\end{bmatrix}.\end{aligned}\tag{41}$$

From (41) it can be seen that using our choice of r_d results in yaw angle error dynamics that have a term dependent on the yaw rate error $\tilde{r}$ and a perturbing term that vanishes when the estimation errors $\tilde{V}_T$ and $\tilde{V}_N$ go to zero. To add acceleration feedforward to the yaw rate controller, the derivative of r_d should be calculated. From the definition of r_d, it can be seen that r_d has the following dependencies $r_d = r_d(h^T, y_{b/p}, x_{b/p}, \tilde{\psi}, \tilde{x}, \tilde{y})$ with $h \triangleq [\theta, v_r, u_r, u_{rd}, \dot{u}_{rd}, \hat{V}_T, \hat{V}_N]^T$ a vector that contains all the variable, whose time derivative do not depend on $\tilde{V}_N$ and $\tilde{V}_T$. However, the other dependencies of r_d do introduce new terms depending on $\tilde{V}_N$ and $\tilde{V}_T$ when the acceleration feedforward is calculated. Consequently, we instead define our yaw rate controller with an acceleration feedforward that contains only the known terms from $\dot{r}_d$

$$\begin{aligned}\tau_r =& -F(u_r,v_r,r)+\frac{\partial r_d}{\partial h^T}\dot{h}-k_1\tilde{r}-k_2C_r\tilde{\psi}\\ &+\frac{\partial r_d}{\partial x_{b/p}}\left(-\frac{k_\delta x_{b/p}}{\sqrt{1+x_{b/p}^2}}+y_{b/p}\kappa(\theta)\dot{\theta}\right)\\ &+\frac{\partial r_d}{\partial\tilde{\psi}}C_r\tilde{r}-\frac{\partial r_d}{\partial\tilde{x}}k_x\tilde{x}-\frac{\partial r_d}{\partial\tilde{y}}k_y\tilde{y}\\ &-\frac{\partial r_d}{\partial y_{b/p}}\left(\frac{u_{td}y_{b/p}}{\sqrt{\Delta^2+(y_{b/p}+g)^2}}-G_1(\cdot)+x_{b/p}\kappa(\theta)\dot{\theta}\right)\end{aligned}\tag{42}$$

where $k_1 > 0$ and $k_2 > 0$ are constant controller gains.

Using the controller (42) in (3f) the yaw rate error dynamics become

$$\begin{aligned}\dot{\tilde{r}} =& -k_1\tilde{r} - k_2C_r\tilde{\psi} + \tfrac{\partial r_d}{\partial \tilde{x}}\tilde{V}_x + \tfrac{\partial r_d}{\partial \tilde{y}}\tilde{V}_y \\ &- \tfrac{\partial r_d}{\partial \tilde{\psi}}\left[\tfrac{2\Delta}{\Delta^2+(y_{b/p}+g)^2}\left[\tfrac{1}{2}+\tfrac{\partial g}{\partial c}y_{b/p}+\tfrac{\partial g}{\partial b}\hat{V}_N\right]\tilde{V}_N \right. \\ &\left. + \tfrac{2\Delta^2\partial g/\partial c-(y_{b/p}+g)}{\Delta^2+(y_{b/p}+g)^2}\tfrac{\partial \Delta}{\partial \boldsymbol{p}_{b/p}}\tfrac{\tilde{V}_T}{\tilde{V}_N}\right] - \tfrac{\partial r_d}{\partial \boldsymbol{p}_{b/p}}\tfrac{\tilde{V}_T}{\tilde{V}_N}\end{aligned} \tag{43}$$

which contains two stabilizing terms $-k_1\tilde{r}$ and $-k_2C_r\tilde{\psi}$, and perturbing terms depending on $\tilde{V}_T$ and $\tilde{V}_N$ that cannot be cancelled by the controller.

Remark 3. It is straightforward to verify that all the terms in (39) are smooth fractionals that are bounded with respect to $(y_{b/p}, x_{b/p}, \tilde{x}, \tilde{y}, \tilde{\psi}, \Delta)$ or are periodic functions with linear arguments, and consequently the partial derivatives in (42) and (43) are all bounded. This is something that is used when showing closed-loop stability in the next section.

6. Closed-loop analysis

In this section we analyze the closed-loop system of the model (3) with controllers (12) and (42) and observer (14), when the frame propagates along the path P with update law (9). To show that the path following is achieved we have to show that $x_{b/p}$ and $y_{b/p}$ converge to zero, and the closed-loop error dynamics of $\tilde{u}$, $\tilde{\psi}$, and $\tilde{r}$ also converge to zero. However, for the sway velocity, since we consider general curved paths, the best hope is to be able to show global boundedness. Since the observer and the surge velocity dynamics converge independently of the other variables, we define two sets of variables: $\tilde{X}_1 \triangleq [y_{b/p}, x_{b/p}, \tilde{\psi}, \tilde{r}]^T$ and $\tilde{X}_2 \triangleq [\tilde{x}, \tilde{y}, \tilde{V}_x, \tilde{V}_y, \tilde{u}]^T$ where $\tilde{X}_2$ contains all the variables that converge to zero independently of the others. Moreover, while the variables $\tilde{X}_1$ and $\tilde{X}_2$ should converge to zero, the sway velocity is required to remain bounded.

To show that the error variables in $\tilde{X}_1$ and $\tilde{X}_2$ converge to zero, we consider the closed-loop system:

$$\begin{aligned}\dot{\tilde{X}}_1 =& \begin{bmatrix} \frac{-u_{td}y_{b/p}}{\sqrt{\Delta^2+(y_{b/p}+g)^2}} - x_{b/p}\kappa(\theta)\dot{\theta} + G_1(\cdot) \\ \frac{-k_\delta x_{b/p}}{\sqrt{1+x_{b/p}^2}} + y_{b/p}\kappa(\theta)\dot{\theta} \\ C_r\tilde{r} \\ -k_1\tilde{r} - k_2C_r\tilde{\psi} \end{bmatrix} \\ &+ \begin{bmatrix} \tilde{V}_N \\ \tilde{V}_T \\ G_2(\Delta, y_{b/p}, x_{b/p}, g, \hat{V}_N, \hat{V}_T, \tilde{V}_N, \tilde{V}_T) \\ -\frac{\partial r_d}{\partial \tilde{\psi}}G_2(\cdot) - \frac{\partial r_d}{\partial \boldsymbol{p}_{b/p}}\frac{\tilde{V}_T}{\tilde{V}_N} + \frac{\partial r_d}{\partial \tilde{x}}\tilde{V}_x + \frac{\partial r_d}{\partial \tilde{y}}\tilde{V}_y \end{bmatrix}\end{aligned} \tag{44a}$$

$$\dot{\tilde{X}}_2 = \begin{bmatrix} -k_{x_1}\tilde{x} - \tilde{V}_x \\ -k_{y_1}\tilde{y} - \tilde{V}_y \\ -k_{x_2}\tilde{x} \\ -k_{y_2}\tilde{y} \\ -k_u\tilde{u} \end{bmatrix} \tag{44b}$$

$$\begin{aligned}\dot{v}_r =& X(u_{rd}+\tilde{u})r_d(h, y_{b/p}, x_{b/p}, \tilde{\psi}, \tilde{x}, \tilde{y}) \\ &+ X(u_{rd}+\tilde{u})\tilde{r} + Y(u_{rd}+\tilde{u})v_r\end{aligned} \tag{44c}$$

where

$$\begin{aligned}G_2(\cdot) =& \tfrac{2\Delta}{\Delta^2+(y_{b/p}+g)^2}\left[\tfrac{1}{2}+\tfrac{\partial g}{\partial c}y_{b/p}+\tfrac{\partial g}{\partial b}\hat{V}_N\right]\tilde{V}_N \\ &+ \tfrac{2\Delta^2\partial g/\partial c-(y_{b/p}+g)}{\Delta^2+(y_{b/p}+g)^2}\tfrac{\partial \Delta}{\partial \boldsymbol{p}_{b/p}}\tfrac{\tilde{V}_T}{\tilde{V}_N}.\end{aligned} \tag{45}$$

Note that $G_2(\Delta, y_{b/p}, x_{b/p}, g, \hat{V}_N, \hat{V}_T, \tilde{V}_N, \tilde{V}_T)$ satisfies

$$\begin{aligned}&G_2(\Delta, y_{b/p}, x_{b/p}, g, \hat{V}_N, \hat{V}_T, 0, 0) = 0 \\ &\|G_2(\cdot)\| \le \zeta_2(\Delta)\|[\tilde{V}_T, \tilde{V}_N]\|,\end{aligned}$$

where $\zeta_2(\Delta) > 0$.

We design the time-varying look-ahead distance as

$$\Delta(x_{b/p}, y_{b/p}) = \sqrt{\mu + x_{b/p}^2 + y_{b/p}^2} \tag{46}$$

where $\mu > 0$ is a constant. Choosing Δ to depend on $x_{b/p}$ and $y_{b/p}$ is necessary to find a bounded value of μ to assure local boundedness of v_r with respect to $\tilde{X}_2$ independently of $\tilde{X}_1$. This shows that $G_2(\cdot)$ is zero when the perturbing variables, i.e. $\tilde{V}_T$ and $\tilde{V}_N$, are zero and $\zeta_2(\Delta)$ has at most linear growth with respect to $x_{b/p}$ and $y_{b/p}$.

The following three steps are taken by formulating and proving three lemmas. For the sake of brevity in the main body of this paper, the proofs of the following lemmas are replaced by a sketch of each proof in the main body. The full proofs can be found in Belleter, Maghenem, Paliotta, and Pettersen (2018).

The first step in the stability analysis of (44) is to assure that the closed-loop system is forward complete and that the sway velocity v_r remains bounded. Therefore, under the assumption that Condition 1 is satisfied, i.e. $C_r > 0$, we take the following three steps:

(1) First, we prove that the trajectories of the closed-loop system are forward complete.
(2) Then, we derive a necessary condition such that v_r is locally bounded with respect to $(\tilde{X}_1, \tilde{X}_2)$.
(3) Finally, we establish that for a sufficiently big value of μ, v_r is locally bounded only with respect to $\tilde{X}_2$, i.e. independently of $\tilde{X}_1$.

Lemma 1 (*Forward Completeness*)**.** *The trajectories of the closed-loop system (44) are forward complete.*

The proof of this lemma is given in Belleter et al. (2018). The general idea is as follows. Forward completeness for (44b) is evident since this part of the closed-loop system consists of GES error dynamics. Using the forward completeness and in fact boundedness of (44b), we can show forward completeness of (44c), $\dot{\tilde{\psi}}$, and $\dot{\tilde{r}}$. Hence, forward completeness of (44) depends on forward completeness of $\dot{x}_{b/p}$ and $\dot{y}_{b/p}$. To show forward completeness of $\dot{x}_{b/p}$ and $\dot{y}_{b/p}$, we consider the $x_{b/p}$ and $y_{b/p}$ dynamics with $\tilde{X}_2$, $\tilde{\psi}$, $\tilde{r}$, and v_r as inputs which allow us to show forward completeness of $\dot{x}_{b/p}$ and $\dot{y}_{b/p}$ according to Angeli and Sontag (1999, Corollary 2.11). Consequently, all the states of the closed-loop system are forward complete, and hence the closed-loop system (44) is forward complete.

Lemma 2 (*Boundedness Near* $(\tilde{X}_1, \tilde{X}_2) = 0$)**.** *The system (44c) is bounded near the manifold* $(\tilde{X}_1, \tilde{X}_2) = 0$ *if and only if the curvature of P satisfies the following condition:*

$$\kappa_{\max} \triangleq \max_{\theta\in P}|\kappa(\theta)| < \frac{Y_{\min}}{2X_{\max}} \quad X_{max} \triangleq |X(u_r)|_\infty. \tag{47}$$

The proof of this lemma is given in Belleter et al. (2018). A sketch of the proof is as follows. The sway velocity dynamics (44c) are analyzed using a quadratic Lyapunov function $V = 1/2v_r^2$. It can be shown that the derivative of this Lyapunov function satisfies

the conditions for boundedness when the solutions are on or close to the manifold where $(\tilde{X}_1, \tilde{X}_2) = 0$. Consequently, (44c) satisfies the conditions of boundedness near $(\tilde{X}_1, \tilde{X}_2) = 0$ as long as (47) is satisfied.

Remark 4. In the proof of Lemma 2 it is shown that choosing $\Delta(x_{b/p}) = \sqrt{\mu + x_{b/p}^2}$ as in Moe et al. (2014), v_r would grow linearly and unbounded with respect to the state $y_{b/f}$. The necessity of choosing Δ as in (46), i.e. Δ dependent also on $y_{b/f}$, is shown and justified.

In Lemma 2 we show boundedness of v_r for small values of $(\tilde{X}_1, \tilde{X}_2)$ to derive the bound on the curvature. However, locality with respect to $\tilde{X}_1$, i.e. the path-following errors and yaw angle and yaw rate errors, is not desirable, and in the next lemma boundedness independent of $\tilde{X}_1$ is shown under an extra condition on the constant μ from the definition (46) of the look-ahead distance Δ.

Lemma 3 (*Boundedness Near $\tilde{X}_2 = 0$*)**.** *The system (44c) is bounded near the manifold $\tilde{X}_2 = 0$, independently of $\tilde{X}_1$, if we choose*

$$\mu > \frac{8X_{\max}}{Y_{\min} - 2X_{\max}\kappa_{\max}} \tag{48}$$

where $X_{max} = |X(u_r)|_\infty$ and $\kappa_{\max} = \max_{\theta\in P} |\kappa(\theta)|$.

The proof of this lemma is given in Belleter et al. (2018). It follows along the same lines of the proof of Lemma 2. That is, when the solutions are close to the manifold $\tilde{X}_2 = 0$, rather than $(\tilde{X}_1, \tilde{X}_2) = 0$, the boundedness can still be shown provided that (48) is satisfied additionally to the conditions of Lemma 2.

Theorem 1. *Consider a θ-parametrized path denoted by $P(\theta) \triangleq (x_p(\theta), y_p(\theta))$, with the update law given by (33). Then under Condition 1 and the conditions of Lemmas 1–3, the system (3) with control laws (12) and (42) and observer (14) follows the path P, while maintaining v_r, τ_r, and τ_u bounded. In particular, the origin of the system (44a)–(44b) is GAS and LES.*

Proof. From the fact that the origin of (44b) is GES, the fact that the closed-loop system (44) is forward complete according to Lemma 1, and the fact that solutions of (44c) are locally bounded near $\tilde{X}_2 = 0$ according to Lemma 3, we can conclude that there is a finite time $T > t_0$ after which solutions of (44b) will be sufficiently close to $\tilde{X}_2 = 0$ to guarantee boundedness of v_r.

Having established that v_r is bounded we first analyze the cascade

$$\begin{bmatrix} \dot{\tilde{\psi}} \\ \dot{\tilde{r}} \end{bmatrix} = \begin{bmatrix} C_r\tilde{r} \\ -k_1\tilde{r} - k_2C_r\tilde{\psi} \end{bmatrix} + \begin{bmatrix} G_2(\cdot) \\ \dfrac{\partial r_d}{\partial[\tilde{x},\tilde{y}]^T}\tilde{\boldsymbol{V}}_c - \dfrac{\partial r_d}{\partial\tilde{\psi}}G_2(\cdot) - \dfrac{\partial r_d}{\partial \boldsymbol{p}_{b/p}}\begin{matrix}\tilde{V}_T \\ \tilde{V}_N\end{matrix} \end{bmatrix} \tag{49a}$$

$$\begin{bmatrix} \dot{\tilde{x}} \\ \dot{\tilde{y}} \\ \dot{\tilde{V}}_x \\ \dot{\tilde{V}}_y \\ \dot{\tilde{u}} \end{bmatrix} = \begin{bmatrix} -k_{x_1}\tilde{x} - \tilde{V}_x \\ -k_{y_1}\tilde{y} - \tilde{V}_y \\ -k_{x_2}\tilde{x} \\ -k_{y_2}\tilde{y} \\ -k_u\tilde{u} \end{bmatrix}. \tag{49b}$$

The perturbing system (49b) is GES as shown in Section 5.2. The interconnection term, i.e. the second matrix in (49a), satisfies the linear growth criteria from Panteley and Loría (1998, Theorem 2). More specifically, it does not grow with the states $\tilde{\psi}$ and $\tilde{r}$ since all the partial derivatives of r_d and $G_2(\cdot)$ can respectively be bounded by constants and linear functions of $\tilde{V}_x$ and $\tilde{V}_y$. The nominal dynamics, i.e. the first matrix in (49a), can be analyzed with the following quadratic Lyapunov function:

$$V_{(\tilde{r},\tilde{\psi})} = \frac{1}{2}\tilde{r}^2 + \frac{1}{2}k_2\tilde{\psi}^2 \tag{50}$$

whose derivative along the solutions of the nominal system is given by

$$\dot{V}_{(\tilde{r},\tilde{\psi})} = k_2C_r\tilde{r}\tilde{\psi} - k_1\tilde{r}^2 - k_2C_r\tilde{\psi}\tilde{r} = -k_2\tilde{r}^2 \le 0 \tag{51}$$

which implies that $\tilde{r}$ and $\tilde{\psi}$ are bounded. The derivative of (51) is given by

$$\ddot{V}_{(\tilde{r},\tilde{\psi})} = -2k_1^2\tilde{r}^2 - 2k_1k_2C_r\tilde{\psi}\tilde{r} \tag{52}$$

which is bounded since $\tilde{r}$ and $\tilde{\psi}$ are bounded. This implies that (51) is a uniformly continuous function. Note that the nominal system is non autonomous, since C_r depends on the time-varying signals $u_r, u_{rd}, \Delta, g, a$, which are well-defined due to the forward completeness property. We will thus apply Barbalat's lemma to further investigate the stability of the nominal system. We conclude

$$\lim_{t\to\infty}\dot{V}_{(\tilde{r},\tilde{\psi})} = \lim_{t\to\infty} -k_1\tilde{r}^2 = 0 \;\Rightarrow\; \lim_{t\to\infty}\tilde{r} = 0. \tag{53}$$

Since C_r is persistently exciting, which follows from the fact that C_r is upper bounded and lower bounded by a constant larger than zero, it follows from the expression of the nominal dynamics that

$$\lim_{t\to\infty}\tilde{r} = 0 \;\Rightarrow\; \lim_{t\to\infty}\tilde{\psi} = 0. \tag{54}$$

This implies that the system is globally asymptotically stable, and since the nominal dynamics are linear it follows that the nominal dynamics are globally exponentially stable. Consequently, from the above it follows that the cascade (49) is GES using Angeli, Sontag, and Wang (2000, Definition 2.2) and Panteley and Loría (1998, Theorem 2).

We now consider the following dynamics:

$$\begin{bmatrix} \dot{y}_{b/p} \\ \dot{x}_{b/p} \end{bmatrix} = \begin{bmatrix} -u_{td}\dfrac{y_{b/p}}{\sqrt{\Delta^2 + (y_{b/p}+g)^2}} - x_{b/p}\kappa(\theta)\dot{\theta} \\ -k_\delta\dfrac{x_{b/p}}{\sqrt{1+x_{b/p}^2}} + y_{b/p}\kappa(\theta)\dot{\theta} \end{bmatrix} + \begin{bmatrix} \tilde{V}_N + G_1(\cdot) \\ \tilde{V}_T \end{bmatrix}. \tag{55}$$

Note that we can view the systems (49) and (55) as a cascaded system where the nominal dynamics are formed by the first matrix of (55), the interconnection term is given by second matrix of (55), and the perturbing dynamics are given by (49). As we have just shown, the perturbing dynamics are GES. Using (29) it is straightforward to verify that the interconnection term satisfies the conditions of Panteley and Loría (1998, Theorem 2). We now consider the following Lyapunov function for the nominal system:

$$V_{\boldsymbol{p}_{b/p}} = \tfrac{1}{2}x_{b/p}^2 + \tfrac{1}{2}y_{b/p}^2 \tag{56}$$

whose derivative along the solutions of the nominal system is given by

$$\dot{V}_{\boldsymbol{p}_{b/p}} = \frac{-u_{td}y_{b/p}^2}{\sqrt{\Delta^2 + (y_{b/p}+g)^2}} - \frac{k_\delta x_{b/p}^2}{\sqrt{1+x_{b/p}^2}} \tag{57}$$

is negative definite. The nominal system is thus GAS. Moreover, since it is straightforward to verify that $\dot{V}_{\boldsymbol{p}_{b/p}} \le \alpha V_{\boldsymbol{p}_{b/p}}$ for some constant α dependent on initial conditions, it follows from the comparison lemma (Khalil, 2002, Lemma 3.4) that the nominal

dynamics are also LES. Consequently, the cascaded system satisfies the conditions of Panteley, Lefeber, Loría, and Nijmeijer (1998, Lemma 8) and Panteley and Loría (1998, Theorem 2), and therefore the cascaded system is GAS and LES. This implies that the origin of the error dynamics, i.e. $(\tilde{X}_1, \tilde{X}_2) = (0, 0)$, is globally asymptotically stable and locally exponentially stable.

Remark 5. Note that this proof uses the theory for cascaded systems which is an approach that has also been taken in most previous works concerning this topic. However, the cascaded argument alone would not hold without establishing forward completeness of the closed-loop solutions and some robustness properties with respect to some vanishing variables in the system, see Lemma 1, 2, and 3. This is a caveat in the stability proof of previous works which we have intended to fill here. Moreover, using the cascade (49) this proof shows that the system can be controlled by a yaw rate controller that does not depend on $\dot{\psi}_d$ and consequently does not depend on the ocean current.

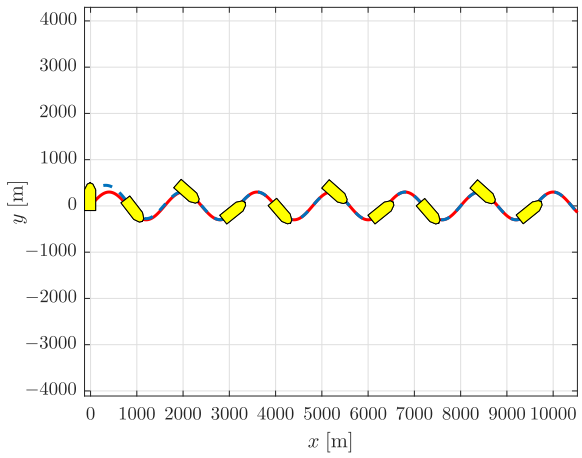

Fig. 3. Path following of the desired sinusoidal path in the $x - y$-plane using the proposed controller.

7. Case study

This section presents two case studies that illustrate the theoretical results presented in this paper. In the first case study, the desired path is a sine curve while in the second case study the ship is requested to follow a path composed of two non-co-linear straight lines (zig-zag path). Moreover, in the latter case, we assume that the ocean current changes direction and magnitude when the ship moves to the second straight-line segment. In both the case studies, we use the parameters values of the underactuated surface vessel studied in Caharija (2014). The vessel considered in Caharija (2014) is an offshore supply vessel equipped with a propeller for thrust and a rudder for yaw actuation. The control input is therefore given by the surge thrust T_u and rudder angle T_r which are allocated as in (1)–(2a).

7.1. Sinusoidal path

The ocean current components are given by $V_x = -0.4$ [m/s] and $V_y = 1$ [m/s] and consequently $V_{\max} \approx 1.08$ [m/s]. The desired relative surge velocity is chosen to be constant and set to $u_{rd} = 5$ [m/s], which means that Assumption 3 is satisfied. We want to remark that a surge speed of 5 [m/s] may be considered as not purely low speed, which could oppose the assumption of linear damping that we made in (1). However, in our simulations we use the damping parameters given in Caharija (2014, Appendix B) which are the result of a linear approximation of the damping term and the approximated linear damping is valid for $|u_r| < 7$ [m/s]. Using the model's parameters given in Caharija (2014), we have $(Y_{\min})/(2X_{\max}) \approx 0.0667$. The observer is initialized as in (17) and the observer gains are selected as $k_{x_1} = k_{y_1} = 1$ and $k_{x_2} = k_{y_2} = 0.1$. The controller gains are selected as $k_{u_r} = 0.1$ for the surge velocity controller and $k_1 = 40$ and $k_2 = 100$ for the yaw rate controller. In this first case study the vessel is required to follow the sinusoidal path $P = \left\{\boldsymbol{p}_{b/p} \in \mathbb{R}^2 : y_{b/p} = 300 \sin\left(\frac{\pi}{800} x_{b/p}\right)\right\}$. Consequently, the maximum curvature of the path is $\max_{\boldsymbol{p}_{b/p} \in P} |\kappa(\theta(x_p))| = 0.0087$. This implies that we satisfy our constraint on the curvature given by Lemma 2 since $\max_{\boldsymbol{p}_{b/p} \in P} |\kappa(\theta(x_p))| < (Y_{\min})/(2X_{\max})$. The required value for μ can be calculated as suggested in Lemma 3 to obtain $\mu > 987.3$ [m], which can be satisfied by choosing $\mu = 1000$ [m]. The initial conditions are

$$[u_r, v_r, r, x, y, \psi]^T = [0, 0, 0, 10, 200, \pi/2]^T. \tag{58}$$

The resulting motion of the ship are shown in Fig. 3. The dashed blue line is the trajectory of the vessel and the red sine curve is the reference. The yellow ship shows the orientation of the ship each 100 [s]. From Fig. 3 it can clearly be seen that the orientation of the ship is not tangent to the sine curve, which is as expected and desired for underactuated vessels in order to compensate for the ocean current. The path-following errors in the tangential direction, $x_{b/p}$, and in the normal direction, $y_{b/p}$ can be seen in the top plot of Fig. 4, from which it can clearly be seen that the path-following errors converge to zero after a transient period. A detail of the last portion of the simulation is given to illustrate that the errors converge to zero. The estimates of the ocean current components obtained from the ocean current observer are given in the second plot from the top in Fig. 4. The previous plot illustrates the conservativeness of the bound $2V_{\max} < u_{rd}(t)$, $\forall t$ derived in the analysis of the observer-error dynamics in Section 5.2. The sway velocity v_r is plotted in the third plot of Fig. 4. This plot shows that due to the curvature of the path, the sway velocity does not converge to zero but remains bounded and follows a periodic motion induced by the periodicity of the desired path which has a curvature that both non-constant and non-zero. The relative surge velocity is plotted in the fourth plot of Fig. 4. This plot clearly shows the exponential convergence of the velocity as it moves to the desired value of $u_{rd} = 5$ [m/s]. Especially interesting is the coupling of the relative surge velocity with the value of C_r in Condition 1. The parameter C_r is plotted in the bottom plot of Fig. 4. From this plot, it can clearly be seen that C_r is bounded away from zero throughout the motion.

7.2. Zig-zag path

In this case study, we assume that the desired path is composed of two linked non-co-linear straight lines, namely $P = P_1 \cup P_2$ where

$$P_1 \triangleq \left\{\boldsymbol{p}_{b/p} \in \mathbb{R}^2 : y_{b/p} = f(x_{b/p}) = x_{b/p},\ \ x_{b/p} \in [0, 1500\ [\text{m}]]\right\}$$

and

$$P_2 \triangleq \left\{\boldsymbol{p}_{b/p} \in \mathbb{R}^2 : y_{b/p} = f(x_{b/p}) = -x_{b/p} + 3000\ [\text{m}],\ x_{b/p} \in [1500\ [\text{m}], 2600\ [\text{m}]]\right\}.$$

When the vessel switches between the paths the ocean current switches as well. That is, when $\boldsymbol{p}_{b/p} \in P_1$, the ocean current components are given by $V_{x1} = -0.4$ [m/s] and $V_{y1} = 1.0$ [m/s] and when the ship maneuvers to follow P_2, $\boldsymbol{p}_{b/p} \in P_2$, the ocean current switches its value to $V_{x2} = -1.0$ [m/s] and $V_{y2} = 0.7$ [m/s]. The simulation with switching current is included to illustrate that

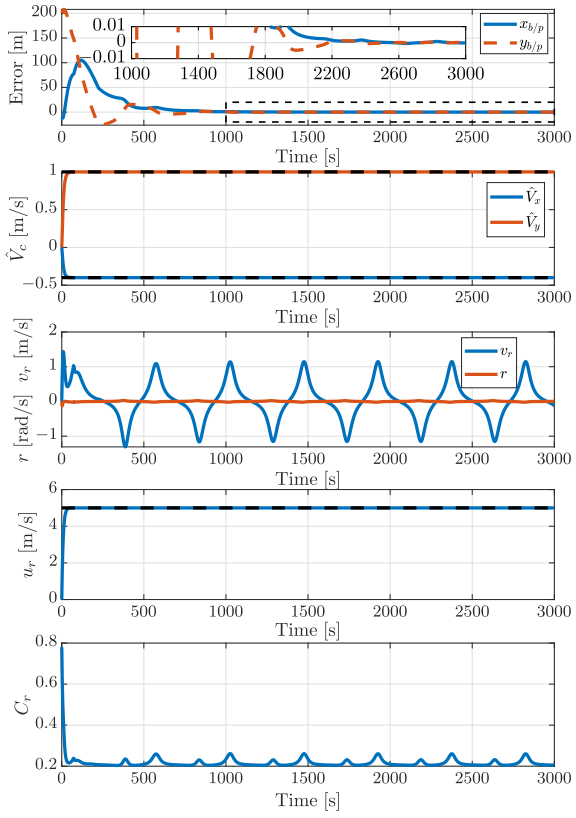

Fig. 4. Time evolution of the path-following errors (top), current estimates (second), sway velocity, yaw rate (third), surge velocity (fourth), and the parameter C_r (bottom).

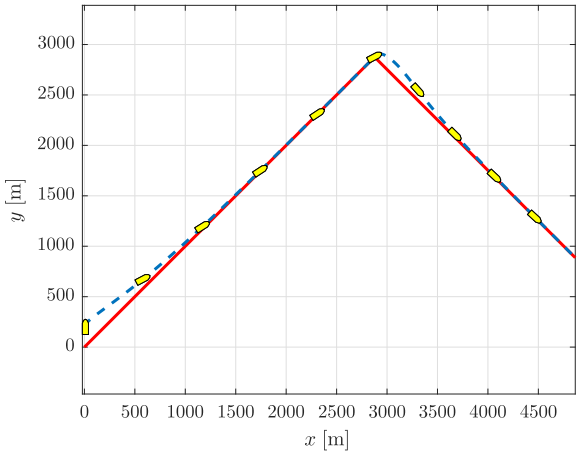

Fig. 5. Path following of the desired zig-zag path in the x-y-plane using the proposed controller.

despite the assumption on the ocean current in Assumption 1, the theoretical analysis and the stability conclusions remain valid when the ocean current is constant at sufficiently large intervals of time and varies only over a finite number of sufficiently small intervals of time. This will allow the observer to adapt and estimate the new value of the ocean during the interval of time where it is constant, and hence the guidance law will be able to control the ship towards the path. With the aforementioned values of the ocean current we have $V_{\max} \approx 1.22$ [m/s]. The desired relative surge velocity is constant with $u_{rd} = 5$ [m/s], which means that Assumption 3 is satisfied. We remark that also for this simulation we use the damping parameters given in Caharija (2014) which give a linear damping term valid for speeds $|u_r| < 7$ [m/s]. The observer's initial condition and gains are the same as in the sinusoidal-path case. The control gains are $k_{u_r} = 0.1$, $k_1 = 40$ and $k_2 = 100$. In this second case study, the vessel is required to follow the path $P \triangleq P_1 \cup P_2$. Consequently, the curvature of the path is equal to zero for almost all $(x_{b/p}, y_{b/p}) \in P$. Hence, our constraint on the curvature $|\kappa(\theta(x_p))| < (Y_{\min})/(2X_{\max}) \approx 0.0087$ is trivially satisfied almost everywhere since $(Y_{\min})/(2X_{\max}) > 0$. Furthermore, according to Lemma 3, we need to satisfy $\mu > 460.9$ [m], which is the case when $\mu = 500$ [m]. The initial conditions are

$$[u_r, v_r, r, x, y, \psi]^T = [0, 0, 0, 10, 200, \pi/2]^T. \tag{59}$$

The resulting motion of the ship can be seen in Fig. 5. The dashed blue line is the trajectory of the vessel and the red line is the reference. The yellow ship shows the orientation of the ship each 100 [s]. From Fig. 5, it can be seen that the ocean current prevents a tangential orientation of the ship with respect to the desired path, which is expected in order to compensate for the ocean current. Furthermore, the estimates for the ocean current components obtained from the ocean current observer are given in the second plot from the top in Fig. 6. From this plot, it can clearly be seen that the estimates converge to the desired value (V_{x1}, V_{y1}). Moreover, when the ocean current switches to (V_{x2}, V_{y2}), the observer shows a short transient behavior before converging to the new value. However, we preserve the conservativeness of the bound $2V_{\max} < u_{rd}(t)$, $\forall t$ derived in the analysis of the observer error dynamics in Section 5.2. Furthermore, during the transient interval during which the observer provides incorrect current estimates to the controller and also due to the switch of the desired-path direction, the path-following errors in the tangential and the normal directions $x_{b/p}$ and $y_{b/p}$, respectively, are affected, as it can be seen from the top plot of Fig. 6. However, it can clearly be seen that the path-following errors converge back to zero after the transient. A detail of the last portions of the simulation is given to illustrate that the errors converge to zero. The sway velocity v_r is plotted in the third plot of Fig. 6. This plot shows that due to the fact that the curvature is zero almost everywhere on the path, the sway velocity converges to zero while the ship moves along the first segment of the path. When the ocean current and the path direction switch, the sway velocity displays a short transient behavior before converging to the origin again. The relative surge velocity is plotted in the fourth plot of Fig. 6 and shows the exponential convergence of the velocity to $u_{rd} = 5$ [m/s]. Furthermore, the evolution of C_r, involved in Condition 1, is plotted in the bottom plot of Fig. 6 where we see that C_r is bounded away from zero throughout the motion.

8. Conclusions

In this work curved-path following for underactuated marine vehicles in the presence of constant ocean currents has been considered. We propose a control approach where the path is parametrized by a path variable with a globally defined update law. The vehicle is steered using a line-of-sight like guidance law where the lookahead-distance depends on the path-following errors. To compensate for the unknown ocean currents, the guidance law is aided by an ocean current observer. The closed-loop system with the controllers and observer was analyzed. This was done by first showing that under certain conditions we have boundedness of the underactuated sway velocity dynamics. Since the paths are curved, the sway velocity will not converge to zero, and boundedness is thus what we aim for. It was then shown that if these conditions are satisfied such that the sway velocity is bounded, the path-following errors are globally asymptotically stable and locally exponentially stable.

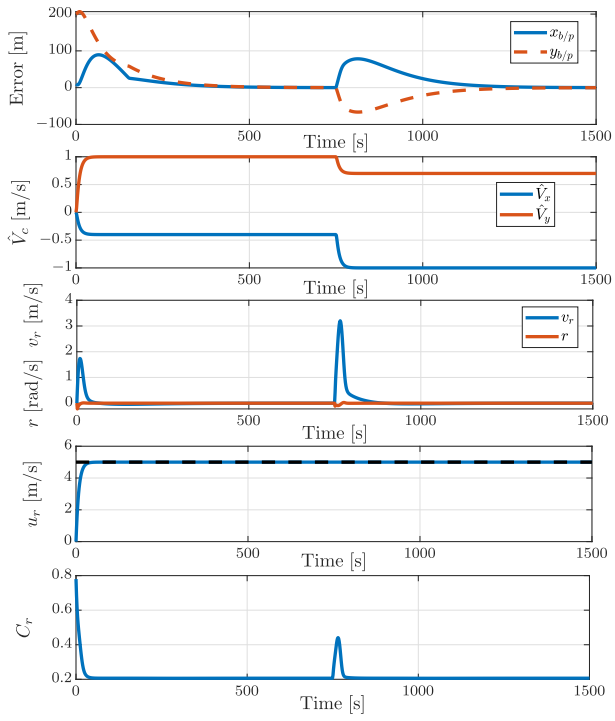

Fig. 6. Time evolution of the path following errors (top), current estimates (second), sway velocity, yaw rate (third), surge velocity (fourth), and magnitude of C_r (bottom).

References

Aguiar, A. P., & Hespanha, J. P. (2007). Trajectory-tracking and path-following of underactuated autonomous vehicles with parametric modeling uncertainty. *IEEE Transactions on Automatic Control*, *52*(8), 1362–1379.

Aguiar, A. P., & Pascoal, A. M. (2007). Dynamic positioning and way-point tracking of underactuated AUVs in the presence of ocean currents. *International Journal of Control*, *80*(7), 1092–1108.

Angeli, D., & Sontag, E. D. (1999). Forward completeness, unboundedness observability, and their lyapunov characterizations. *Systems & Control Letters*, *38*(4), 209–217.

Angeli, D., Sontag, E. D., & Wang, Y. (2000). A characterization of integral input-to-state stability. *IEEE Transactions on Automatic Control*, *45*(6), 1082–1097.

Belleter, D.J.W., Maghenem, M., Paliotta, C., & Pettersen, K.Y. (2018). Observer based path following for underactuated marine vessels in the presence of ocean currents: A global approach-with proofs. arXiv preprint arXiv:1810.06974.

Børhaug, E., Pavlov, A., Panteley, E., & Pettersen, K. Y. (2011). Straight line path following for formations of underactuated marine surface vessels. *IEEE Transactions on Control Systems Technology*, *19*(3), 493–506.

Børhaug, E., Pavlov, A., & Pettersen, K. Y. (2008). Integral LOS control for path following of underactuated marine surface vessels in the presence of ocean currents. In *Proc. of the 47th IEEE conference on decision and control* (pp. 4984–4991).

Børhaug, E., & Pettersen, K. Y. (2006). Los path following for underactuated underwater vehicle. In *Proc. of the 7th IFAC conference on manoeuvering and control of marine craft MCMC, Lisbon, Portugal*.

Breivik, M., & Fossen, T. I. (2004). Path following of straight lines and circles for marine surface vessels. In *Proc. of the 6th IFAC control applications in marine systems*.

Breivik, M., & Fossen, T. I. (2005a). Guidance-based path following for autonomous underwater vehicles. In *Proc. of OCEANS 2005 MTS/IEEE* (pp. 2807–2814). IEEE.

Breivik, M., & Fossen, T. I. (2005b). Principles of guidance-based path following in 2d and 3d. In *Proc. of the 44th IEEE conference on decision and control* (pp. 627–634). IEEE.

Caharija, W. (2014). *Integral line-of-sight guidance and control of underactuated marine vehicles* (Ph.D. thesis), Norwegian University of Science and Technology.

Caharija, W., Candeloro, M., Pettersen, K. Y., & Sørensen, A. J. (2012). Relative velocity control and integral los for path following of underactuated surface vessels. In *Proc. of the 9th IFAC conference on manoeuvring and control of marine craft*.

Caharija, W., Pettersen, K. Y., Bibuli, M., Calado, P., Zereik, E., Braga, J., et al. (2016). Integral line-of-sight guidance and control of underactuated marine vehicles: Theory, simulations and experiments. *IEEE Transactions on Control Systems Technology*, *24*(5), 1623–1642.

Caharija, W., Pettersen, K. Y., Gravdahl, J. T., & Børhaug, E. (2012). Path following of underactuated autonomous underwater vehicles in the presence of ocean currents. In *Proc. of the 51th IEEE conference on decision and control* (pp. 528–535).

Do, K. D., & Pan, J. (2004). State-and output-feedback robust path-following controllers for underactuated ships using Serret–Frenet frame. *Ocean Engineering*, *31*(5), 587–613.

Do, K. D., & Pan, J. (2006). Global robust adaptive path following of underactuated ships. *Automatica*, *42*(10), 1713–1722.

Encarnaçao, P., & Pascoal, A. (2000). 3d path following for autonomous underwater vehicle. In *Proc. of the 39th IEEE conference on decision and control*.

Encarnaçao, P., Pascoal, A., & Arcak, M. (2000). Path following for marine vehicles in the presence of unknown currents. In *Proc. of SYROCO 6th IFAC symposium on robot control* (pp. 469–474).

Fossen, T. I. (2011). *Handbook of marine craft hydrodynamics and motion control*. Wiley.

Fossen, T. I., Breivik, M., & Skjetne, R. (2003). Line-of-sight paht following of underactuated marine craft. In *Proc. of the 6th IFAC conference on manoeuvering and control of marine craft* (pp. 244–249).

Fredriksen, E., & Pettersen, K. Y. (2004). Global κ-exponential way-point manoeuvering of ships. In *Proc. of the 43rd IEEE conference on decision and control (CDC)* (pp. 5360–5367). IEEE.

Khalil, H. (2002). *Nonlinear systems*. Prentice Hall.

Lapierre, L., & Soetanto, D. (2007). Nonlinear path-following control of an AUV. *Ocean Engineering*, *34*(11), 1734–1744.

Lapierre, L., Soetanto, D., & Pascoal, A. (2003). Nonlinear path following with applications to the control of autonomous underwater vehicles. In *Proc. of the 42nd IEEE conference on decision and control (CDC)* (pp. 1256–1261). IEEE.

Li, Z., Sun, J., & Oh, S. (2009). Design, analysis and experimental validation of a robust nonlinear path following controller for marine surface vessels. *Automatica*, *45*(7), 1649–1658.

Maghenem, M., Belleter, D. J. W., Paliotta, C., & Pettersen, K. Y. (2017). Observer based path following for underactuated marine vessels in the presence of ocean currents: a local approach. In *Proc. the 55th IFAC world congress, Toulouse, France*.

Micaelli, A., & Samson, C. (1993). *Trajectory tracking for unicycle-type and two-steering-wheels mobile robots* (Ph.D. thesis), INRIA.

Moe, S., Caharija, W., Pettersen, K. Y., & Schjølberg, I. (2014). Path following of underactuated marine surface vessels in the presence of unknown ocean currents. In *Proc. of the American control conference* (pp. 3856–3861). IEEE.

Narendra, K., & Annaswamy, A. (1987). A new adaptive law for robust adaptation without persistent excitation. *IEEE Transactions on Automatic Control*, *32*(2), 134–145.

Oh, S.-R., & Sun, J. (2010). Path following of underactuated marine surface vessels using line-of-sight based model predictive control. *Ocean Engineering*, *37*(2), 289–295.

Paliotta, C., Lefeber, E., Pettersen, Kristin Y., Pinto, J., Costa, M., & Sousa, J. (2018). Trajectory tracking and path following for under-actuated marine vehicles. *IEEE Transacations on Control Systems and Technology*.

Panteley, E., Lefeber, E., Loria, A., & Nijmeijer, H. (1998). Exponential tracking control of a mobile car using a cascaded approach. In *Proc. of the IFAC workshop on motion control* (pp. 221–226). Grenoble, France Grenoble, France.

Panteley, E., & Loria, A. (1998). On global uniform asymptotic stability of nonlinear time-varying systems in cascade. *Systems & Control Letters*, *33*(2), 131–138.

Samson, C. (1992). Path following and time-varying feedback stabilization of a wheeled mobile robot. In *Proc. of the international conference on control, automation, robotics and vision*.

Soetanto, D., Lapierre, L., & Pascoal, A. (2003). Adaptive, non-singular path-following control of dynamic wheeled robots. In *Proc. of the 42nd IEEE conference on decision and control(CDC)* (pp. 1765–1770). IEEE.

Dennis Belleter received his M.Sc. degree in Mechanical Engineering from the Eindhoven University of Technology, Eindhoven, The Netherlands in 2013 and his Ph.D. degree from the department of Engineering Cybernetics of the Norwegian University of Science and Technology, Trondheim, Norway in 2016. During this period he has been active in the fields of control of underactuated systems, control of nonlinear mechanical systems, control of marine systems, path-following control and frequency estimation.

He is currently employed at Bosch Rexroth B.V. in the Netherlands as a Design Engineer Dynamics and Control. In this role he works on dynamical analysis and control design for motion simulation and compensation systems.

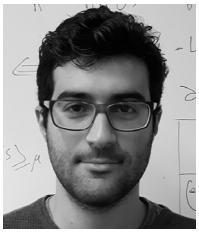

Mohamed Adlene Maghenem received his Control-Engineer degree from the Polytechnical School of Algiers, Algeria, in 2013, his M.S. and Ph.D. degrees in Control from the University of Paris-Saclay, France, in 2014 and 2017, respectively. He is currently a Postdoctoral Fellow at Electrical and Computer Engineering Department at the University of California, Santa Cruz.

His research interests include distributed coordination of multiagent systems, synchronization of oscillators, nonholonomic and underactuated systems, and hybrid dynamical systems.

Claudio Paliotta received his M.Sc. in Mechanical Engineering from the University of Cassino and Southern Latium, Cassino, Italy, in 2013. In 2017 he received his Ph.D. in Engineering Cybernetics from the Norwegian University of Science and Technology, Trondheim, Norway. During the Ph.D., he has carried out research on topics like path following control, trajectory tracking control, synchronization and coordination control of autonomous marine vehicles. He is currently working at Volvo GTT, Gothenburg, Sweden, as Lead Embedded Application Engineer. In this role, he is developing functionalities and software for longitudinal and lateral stability of ground vehicles.

Kristin Y. Pettersen is a Professor in the Department of Engineering Cybernetics, NTNU where she has been a faculty member since 1996. She was Head of Department 2011–2013, Vice-Head of Department 2009–2011, and Director of the NTNU ICT Programme of Robotics 2010–2013. She is Adjunct Professor at the Norwegian Defence Research Establishment (FFI). In the period 2013–2022 she is also Key Scientist at the CoE Centre for Autonomous Marine Operations and Systems (NTNU AMOS). She is a co-founder of the NTNU spin-off company Eelume AS, where she was CEO 2015–2016

She received the M.Sc. and Ph.D. degrees in Engineering Cybernetics at NTNU, Trondheim, Norway, in 1992 and 1996, respectively. She has published four books and more than 25 papers in scientific conferences and journals. Her research interests focus on nonlinear control of mechanical systems with applications to robotics, with a special emphasis on marine robotics and snake robotics. She was awarded the IEEE Transactions on Control Systems Technology Outstanding Paper Award in 2006 and in 2017.

She is a member of the IFAC Council and was a member of the Board of Governors of IEEE Control Systems Society 2012–2014. She has also held and holds several board positions in industrial and research companies. She is an IEEE Fellow, member of the Norwegian Academy of Technological Sciences, and member of the Academy of the Royal Norwegian Society of Sciences and Letters.